Giant nonlinear magneto-optical Kerr effects from Fe interfaces (invited)

Th. Rasing, M. Groot Koerkamp, and B. Koopmans[a)]
Research Institute for Materials, University of Nijmegen, Toernooiveld 1, NL-6525 ED Nijmegen, The Netherlands

H. v.d. Berg
Siemens AG, D-91052 Erlangen, Germany

Second harmonic generation from magnetic materials is shown to lead to a nonlinear magneto-optical Kerr effect that can be orders of magnitude larger than its linear equivalent. The origin of this effect can be found in the differences between the linear and nonlinear solutions of the optical wave equations and in the symmetry properties of the corresponding optical tensors. Applications for the study of magnetic surfaces, thin films, and multilayers will be discussed.
 [S0021-8979(96)13108-X]

I. INTRODUCTION

When linearly polarized light is incident on a magnetic material, the reflected beam will be elliptically polarized, with the major axis of the polarization ellipse rotated with respect to the incident plane of polarization. The origin of this magneto-optical Kerr effect (MOKE) lies in the spin-orbit coupling that leads to a difference in the refraction coefficient for left- and right-handed circularly polarized light. This spin-orbit coupling acts like a magnetic field on the current induced by the electromagnetic field of the incident light.[1] This should also hold for the nonlinear contributions of the induced current, that are the origin of optical second harmonic generation (SHG), leading to a nonlinear magneto-optical Kerr effect (NOMOKE). Based on symmetry arguments, Ru-Pin Pan *et al.* indeed showed that the presence of a magnetization would lead to new, nonzero *surface* contributions to the nonlinear optical response.[2] At the same time, Hübner and Bennemann calculated the nonlinear magneto-optical spectrum of Ni, based on a spin dependent band structure calculation.[3] They showed that this should indeed lead to observable effects, with magnetic contributions to the nonlinear tensor coefficients of more than 10%. First experimental evidence for such a NOMOKE was given by Reif *et al.* for an Fe(110) surface,[4] whereas Spierings *et al.* showed the first NOMOKE results from buried Co/Au interfaces.[5] From a SHG study of $Y_{2.5}Bi_{0.5}Fe_5O_{12}$ films, Aktsipetrov *et al.* reported a nonlinear Kerr rotation between 1° and 4°, that was significantly larger than the linear one.[6] These observations triggered much theoretical and experimental research. Reif *et al.* showed the presence of a magnetic circular dichroism in the SHG reflection from the Heussler alloy PtMnSb, as well as a large nonlinear Kerr rotation of 14°,[7] which is an order of magnitude larger than its linear Kerr angle of 1.1°. Interface and monolayer sensitivity was successfully demonstrated by Wierenga *et al.*[8,9] and nonlinear circular dichroism by Fiebig *et al.*,[10] whereas enormous enhancements of the nonlinear Kerr rotation were observed for a thin Fe/Cr film by Koopmans *et al.*[11] Theoretically, these large enhancements appeared to follow from the differences in the solutions for the Maxwell equations for the nonlinear and linear case,[12] and the differences in the symmetry properties of the linear and nonlinear susceptibilities.[11] In combination with the intrinsic surface and interface sensitivity of the SHG response[13] these large NOMOKE effects are particularly interesting for the study of surface magnetism.

SHG arises from the nonlinear polarization $\mathbf{P}(2\omega)$ induced by an incident laser field $\mathbf{E}(\omega)$. This polarization can be written as an expansion in $\mathbf{E}(\omega)$

$$\mathbf{P}(2\omega)=\boldsymbol{\chi}^{(2)}\mathbf{E}(\omega)\mathbf{E}(\omega)+\boldsymbol{\chi}^{(3)}\mathbf{E}(\omega)\nabla\mathbf{E}(\omega)+\cdots . \quad (1)$$

The lowest order term in Eq. (1) describes an electric dipole source. Symmetry considerations show that this contribution is zero in a centrosymmetric medium, thus limiting electric dipole radiation to the interfaces where inversion symmetry is broken. The bulk second harmonic can now be described in terms of the much smaller electric quadrupolelike contributions [second term in Eq. (1)]. However, because of the large volume difference between interface and bulk, this does not necessarily mean that the total bulk second harmonic signal is negligible. Interface sensitivity needs to be verified for any given system. Following the approach of Pan, Wei, and Shen,[2] it is convenient to separate the SH susceptibility into an even (χ^+) and an odd (χ^-) part in the magnetization $\mathbf{M}$. Thus, the induced SH polarization at an interface $\mathbf{P}(2\omega)$ is given by

$$P_i(2\omega)=\chi^{+}_{ijk}(\mathbf{M})E_jE_k+\chi^{-}_{ijk}(\mathbf{M})E_jE_k, \quad (2)$$

where $\mathbf{E}$ is the local excitation field at frequency ω at the interface, and we implicity assumed a summation over the repeated indices. The introduced susceptibilities fulfill $\chi^{\pm}_{ijk}(-\mathbf{M})=\pm\chi^{\pm}_{ijk}(\mathbf{M})$. In the following we will drop the ex-

TABLE I. The nonzero elements of the SH susceptibility tensor for an isotropic surface in the longitudinal configuration ($\mathbf{M}//\hat{x}$). The two columns list the elements that are even and odd in the magnetization, respectively. The occurrence of the elements in the p- and s-input configuration is indicated within parenthesis.

χ^+		χ^-	
zxx	(p)	yxx	(p)
zyy	(s)	yyy	(s)
zzz	(p)	yzz	(p)
$xzx=xxz$	(p)	$zyz=zzy$	
$yzy=yyz$		$xyx=xxy$	

[a)]Present address: Max Planck Institut für Festkörperforschung, D-70506 Stuttgart, Germany.

 0021-8979/96/79(8)/6181/5/$10.00

plicit **M** dependence of $\chi^{\pm}_{ijk}$. For a given surface symmetry the χ^{+}_{ijk} and χ^{-}_{ijk} can be easily derived (see Table I). In the longitudinal configuration and for pure p- or s-input polarization we find that all nonzero χ^{+}_{ijk} elements have $i \epsilon \{x,z\}$, giving rise to p-polarized SHG. All nonzero χ^{-}_{ijk} elements have $i=y$, always resulting in s-polarized SHG. From this it follows that the SHG polarization ellipses for $\pm\mathbf{M}$ are each other's mirror image in the plane of incidence, and we can define a nonlinear Kerr angle $\Phi^{(2)}_K$ in correspondence with its linear counterpart $\Phi^{(1)}_K$. Pustogowa and Hübner have shown that for the longitudinal configuration $\Phi^{(2)}_K$ and $\Phi^{(1)}_K$ are given by

$$\tan \Phi^{(2)}_K = i\left[\frac{\chi^{(2),-}}{\chi^{(2),+}} + (h.o.)\right] \tag{3}$$

$$\tan \Phi^{(1)}_K \approx -\frac{\chi^{(1)-}}{\chi^{(1)+}} \frac{\sin\theta_i \cos\theta_i}{\sqrt{\cos^2\theta_i + \chi_0(\omega)}} \tag{4}$$

in which $\chi^{(1),+}$ and $\chi^{(1),-}$ are the nonmagnetic and magnetic contributions to $\chi^{(1)}$. The big difference between the expressions for $\Phi^{(2)}_K$ and $\Phi^{(1)}_K$ is the factor $1/\sqrt{\cos^2\theta_i+\chi_0(\omega)}$ in Eq. (4). This factor causes a small value for $\Phi^{(1)}_K$ but is not present in the nonlinear case. Therefore it is clear that the nonlinear Kerr rotation for all θ_i is always enhanced by a factor $\sqrt{\cos^2\theta_i+\chi_0(\omega)}$. Above this effect, in the nonlinear case one can select large magnetic $\chi^{(2)}$ contributions by a proper choice of input polarization and angle of incidence. This is in contrast with the linear case where one always deals with small off-diagonal magnetic terms $[\chi^{-}(\omega)]$ relative to large diagonal nonmagnetic terms $[\chi^{+}(\omega)]$.

II. EXPERIMENTAL RESULTS AND ANALYSIS

The experiments on the nonlinear Kerr rotation from thin, centrosymmetric magnetic films were stimulated by the prediction of large enhancements of $\Phi^{(2)}_K$ by Pustogowa and Hübner.[12] To enable direct comparison with their theoretical results, experiments were performed on Fe thin films and single crystals. All experiments were done *ex situ* and, therefore, required protective cover layers. The first sample consisted of a thin Fe film (thickness 2 nm), covered with a 2 nm Cr film deposited by rf-diode and dc magnetron sputtering, respectively. As a substrate we used a (100) silicon wafer, with a thermal oxide layer of about 525 nm. The substrate was on a rotating table, which moved with a velocity of 0.96 and 3.97 m/min underneath the Fe and Cr targets, respectively. Both targets were equipped with screens for getting uniformity of the layer thickness better than 1%. The base pressure was 2×10^{-7} Torr and the Ar pressure was 5 mTorr. For the second harmonic experiments we used the 770 nm output of a mode-locked (80 MHz) Ti–sapphire laser. The pulse width was 70 fs and the input power was 100 mW focused on a spot diameter of 100 μm. The experiments were done in the longitudinal configuration, i.e., the magnetization **M** was in the plane of the sample and in the optical plane of incidence (see inset Fig. 1). Figure 1 shows the polarization dependence of the SH signal for an s-polarized input at an angle of incidence of 45° and for **M** along $\hat{x}$ and $-\hat{x}$ respectively. The difference between the two minima of

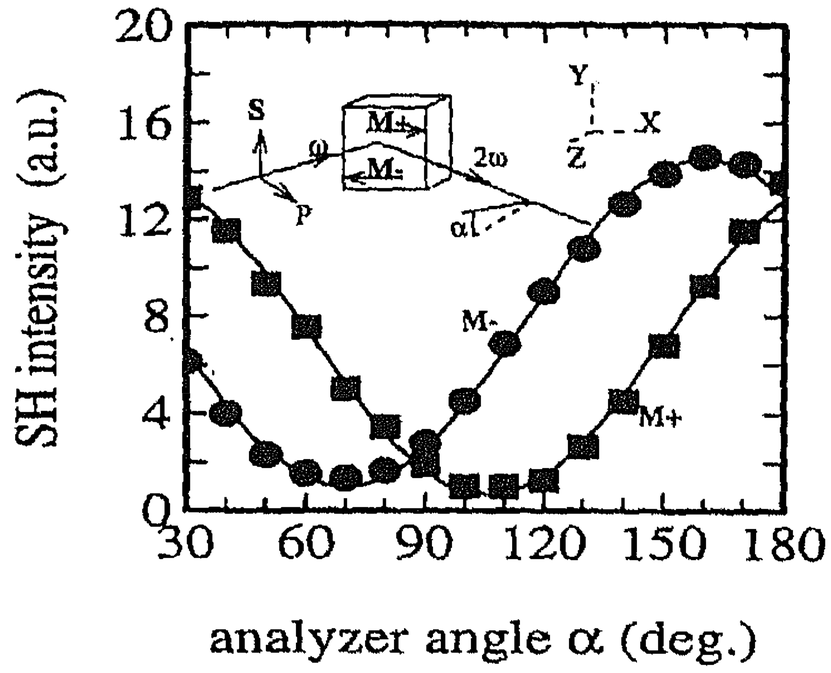

FIG. 1. Output polarization dependence of SHG reflection from an Fe/Cr multilayer, for s-polarized input. Squares: $\mathbf{M}\|\hat{x}$, dots $\mathbf{M}\|-\hat{x}$. The inset shows the experimental configuration.

the curves corresponds to $2\Phi^{(2)}_K \approx 34°$, i.e., a nonlinear Kerr rotation $\Phi^{(2)}_K$ of 17°. In this geometry we measured a linear Kerr angle of 0.03°, using the same Ti–sapphire input beam. These observations correspond to an enhancement of almost *three orders* of magnitude for the nonlinear Kerr rotation! The small linear rotation can be compared with the bulk Fe value of 0.1°.

The nonlinear Kerr angle can be expressed in the s- and p-components of the reflected SH field, denoted by $E_s(2\omega)$ and $E_p(2\omega)$, respectively. The relevant tensor components and their appearance for s- and p-polarized input are shown in Table I. Defining $R \equiv \mathrm{Re}[E_s(2\omega)/E_p(2\omega)]$, $I \equiv \mathrm{Im}[E_s(2\omega)/E_p(2\omega)]$ and $A^2 = R^2 + I^2$ we get

$$\Phi^{(2)}_K = \tfrac{1}{2}\arctan[2R/(1-A^2)] + \phi_0 \tag{5}$$

with $\phi_0=0$ for $A^2 \leqslant 1$, $\phi_0=90°$ for $A^2>1$ and $R \geqslant 0$, and $\phi_0=-90°$ for $A^2>1$ and $R<0$. Equation (5) is completely analogous to expression (3). It is easily verified that in the limit $A \ll 1$ Eq. (5) reduces to $\Phi^{(2)}_K = R$. However, the nonlinear case generally is far from this limit, since $\Phi^{(2)}_K$ can become as large as 90°.

Inspection of Table I shows that the s-input configuration is particularly simple, with only one even, χ^{+}_{zyy}, and one odd, χ^{-}_{yyy}, contributing element per interface. For normal incidence, only the χ^{-}_{yyy} contribution survives. From $E_p(2\omega)=0$ we then find $\Phi^{(2)}_K = \pm 90°$. Moving away from normal incidence, the ratio $|E_s(2\omega)/E_p(2\omega)|$ and, as a consequence, $|\Phi^{(2)}_K|$ decreases so that $\Phi^{(2)}_K$ is tunable over a wide range while scanning the angle of incidence.

A similar argument for a large $\Phi^{(2)}_K$ close to normal incidence is found for a p-polarized input configuration. Table I shows that close to normal incidence, the dominating even tensor components have one z index, and thus vanish at normal incidence, whereas the dominant odd tensor element, χ^{-}_{yxx}, is finite at normal incidence.

Fig. 2 shows the observed nonlinear Kerr rotation for both s- and p-polarized input as a function of the angle of incidence. We observed a small in-plane anisotropy in our experimental results that is possibly induced by the sputtering process. The plotted data in Fig. 2 have been averaged over this azimuthal anisotropy. The solid curves in Fig. 2 are theoretical fits, based on the multiple reflection model, with

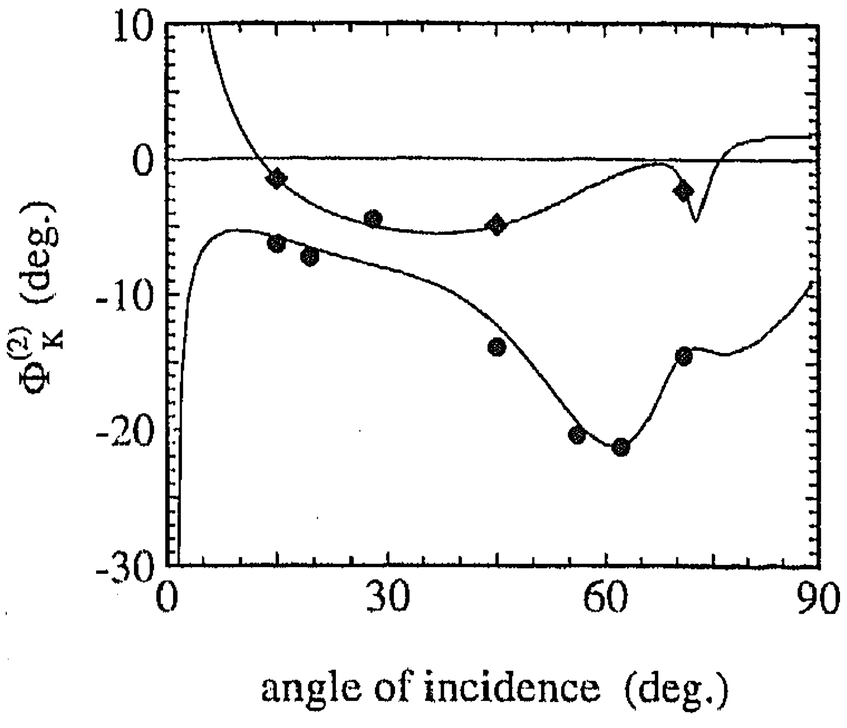

FIG. 2. Nonlinear Kerr rotation $\Phi_K^{(2)}$ for an Fe/Cr multilayer as a function of the angle of incidence. Dots: *s*-input polarization, diamonds: *p*-input polarization. The curves are theoretical fits.

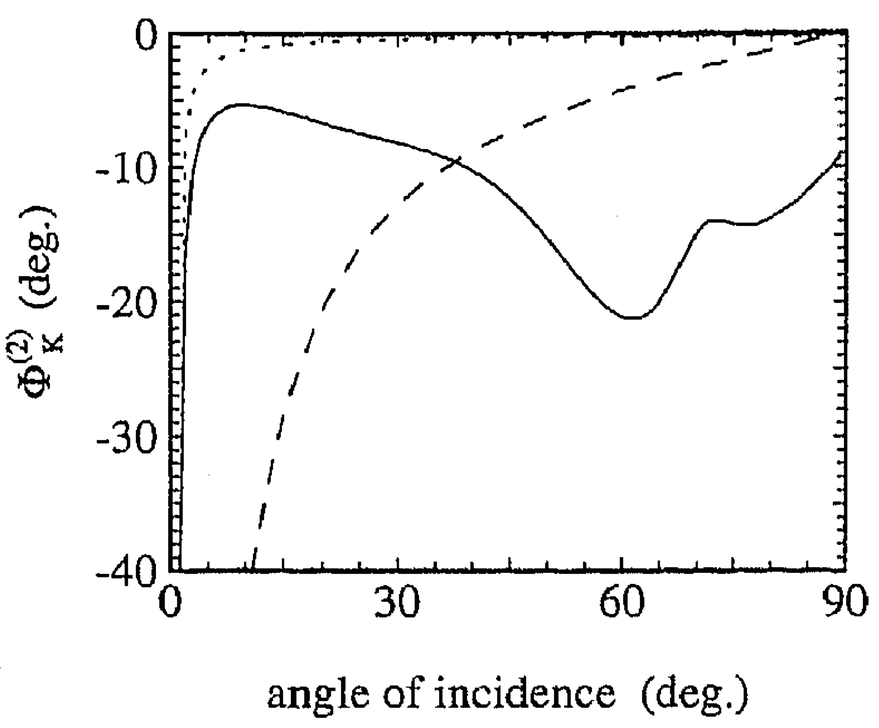

FIG. 3. Nonlinear Kerr rotation $\Phi_K^{(2)}$ for an Fe/Cr multilayer and a bulk Fe surface for *s*-polarized input as a function of the angle of incidence. The bold solid line is the theoretical fit of Fig. 2. The dashed line is a simulation for $\Phi_K^{(2)}$ of a clean Fe surface, based on the multilayer fit. The dotted line is a simulation for $\Phi_K^{(2)}$ for an Fe/Cr multilayer on a silicon wafer with a 10 nm oxide.

the unknown interface tensor elements of Table I as parameters and the following assumptions. Only the Fe is expected to contribute to the magnetic (odd) nonlinear susceptibility because the Cr film is antiferromagnetic. Furthermore, the top Cr layer will be oxidized, so that the major contribution to the nonmagnetic nonlinear susceptibility is also expected to originate from the Fe film. Therefore we assigned effective SH susceptibilities to the Fe and Cr layer together. We verified that the actual position within the Cr/Fe top layer did not significantly change the results of our fits. In addition to these SH sources at the top layer, we incorporate a nonmagnetic SH source at the Si/oxide interface. The bulk optical constants of the metals and silicon were obtained from Refs. 14 and 15, respectively. Because of the limited number of parameters involved in the *s*-polarization configuration (χ_{yyy}^{-} and χ_{zyy}^{+} at the top layer, and χ_{zyy}^{+} at the Si/oxide interface) one finds a unique fit to these experimental data points. The fit in Fig. 2 includes a relative maximum of $|\Phi_K^{(2)}|$ near $\Theta_i \approx 65°$, that is due to an enhancement effect through multiple reflections in the thick silicon oxide layer. Similar, but smaller, enhancement factors due to a substrate are also known for the linear Kerr angle.[16]

For the *p*-polarization, several combinations of tensor elements give satisfying fits. Figure 2 gives one such solution, obtained by choosing fixed values for the relative phase factors and fitting the absolute values of the tensor components. At 45° angle of incidence, we experimentally find for the *p* input $\Phi_K^{(2)} = 4.9°$.

These results show that for a proper understanding and analysis of the nonlinear response the total electro-magnetic response, linear and nonlinear including multiple reflections, has to be considered. The importance of such substrate effects can be illustrated in the following way. From our thin-film analysis we can simply calculate the response of an Fe surface by letting the thickness of the Fe film go to infinity. Similarly, we can vary the thickness of the silicon oxide layer for the thin-film structure.

Figure 3 shows the results of such simulations. For the thin oxide layer, the enhancement effect around $\theta_i = 60°$ has totally vanished, which demonstrates the importance of the multiple reflections and of the local field effects and thus the role of the substrate.

For the bulk surface, Fig. 3 shows a smooth variation of $\Phi_K^{(2)}$ as a function of the angle of incidence. In accordance with Eq. (5), Fig. 3 shows the $\Phi_K^{(2)}$ can be tuned at will between 0° and 90°, by varying the angle of incidence. This is a direct result of the fact that near normal incidence, the even contribution $\chi_{zyy}^{(2),+}$ vanishes, whereas the odd magnetic term $\chi_{xyy}^{(2),-}$ gives a finite contribution.

The prediction of this large tunable nonlinear Kerr rotation was confirmed by experiments on single crystalline Fe whiskers.[17] The (100) surfaces of the whiskers were capped by molecular beam epitaxy grown Au and Cr layers, while

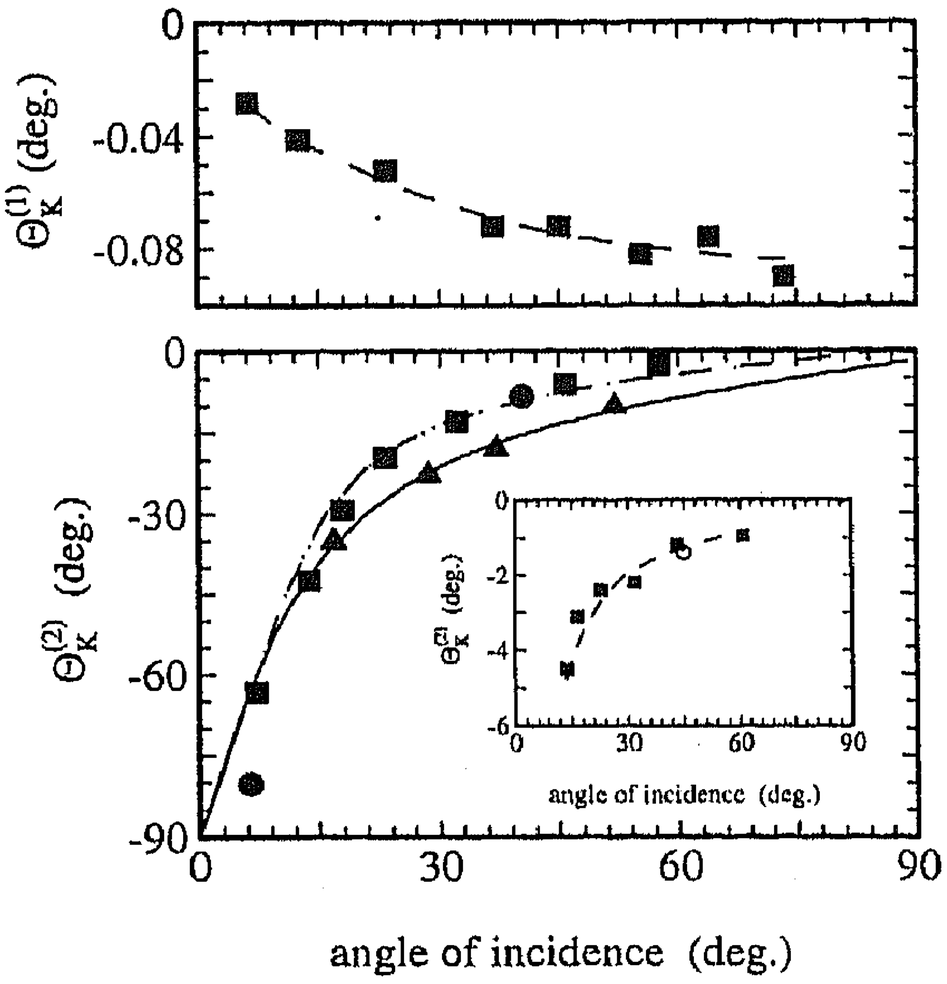

FIG. 4. Linear and nonlinear Kerr rotation for an Fe surface for *s*-polarized input in the longitudinal configuration as a function of the angle of incidence. Triangles: Fe/Cr, Dots: Fe/Au, Squares: uncapped Fe. The solid line is a theoretical fit for the Fe/Cr sample. The dotted line is the theoretical prediction for a clean Fe surface from Ref. 11. The inset shows $\Phi_K^{(2)}$ for *p*-polarized input. The open circle is the calculation from Ref. 12.

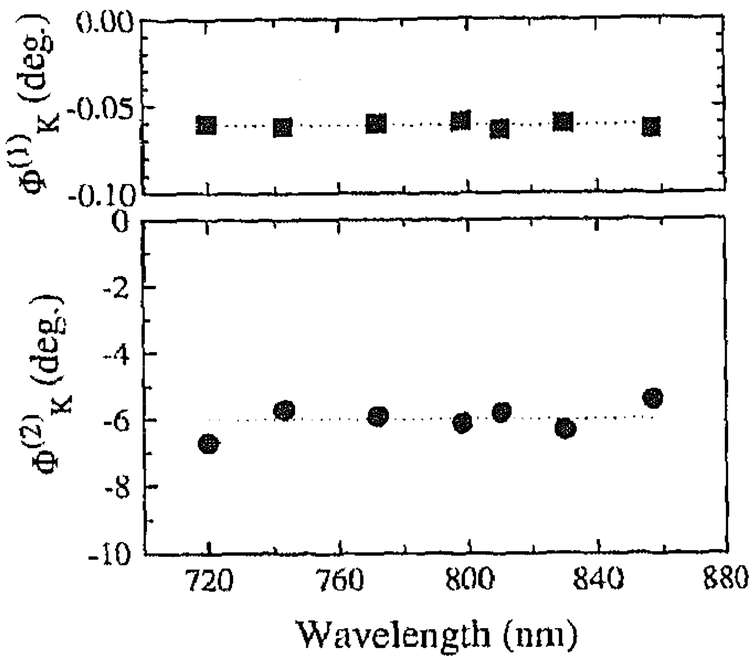

FIG. 5. Experimental wavelength dependence of the nonlinear (dots) and linear (squares) Kerr angle of Fe for the s-input longitudinal configuration at an incident angle of 45°.

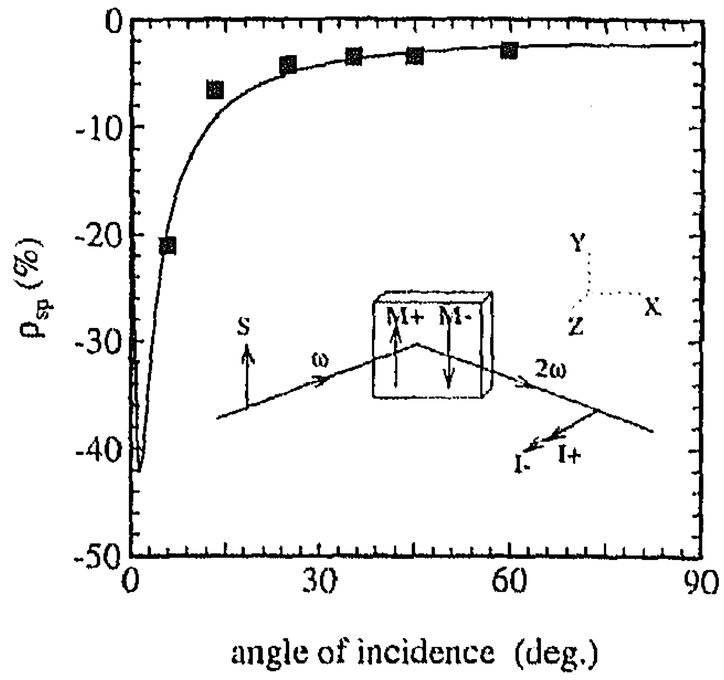

FIG. 6. Magnetic contrast ρ for an uncapped Fe surface for s-polarized input in the transversal configuration as a function of the angle of incidence. The solid line is a theoretical fit. The inset shows the experimental configuration.

some experiments were also performed on uncapped, oxidized Fe whiskers. The experiments were done using the 833 nm output of the Ti–sapphire laser. Figure 4 shows the measured angular dependence of the nonlinear Kerr rotation in the longitudinal configuration and s-polarized excitation. In Fig. 4 the experimental results can be seen for an Fe sample with a Cr top layer, an Fe sample with an Au top layer, and for an uncapped oxidized Fe sample. We find a maximum Kerr angle of 80° at an angle of incidence of 6°. This corresponds to an enhancement of more than a factor 10^3, compared with the value for the linear Kerr rotation of 0.03° as obtained in the same experimental setup, using the fundamental incident beam. The solid line in Fig. 4 is a theoretical fit for the Fe/Cr sample based on Eq. (5) and a model for SHG from interfaces.[18] Furthermore, the experimental results are in quite good agreement with the predicted behavior from Fig. 3.

The inset in Fig. 4 shows the experimental results for the longitudinal configuration with p-polarized incident light. In Table I it can be seen that now we are dealing with two odd tensor components, both of which give rise to s-polarized SHG and three even components which produce p-polarized SHG. Therefore it is to be expected that for the same incidence angles the ratio $|E_s(2\omega)/E_p(2\omega)|$ and thus $\Phi_K^{(2)}$ will be smaller compared to the s-input configuration. Near normal incidence the influence of the components χ_{ijk} with a "z" for i, j, or k will again be small. Since all even tensor components have at least one z index the p-polarized SHG will then be small. The s-polarized SHG, which is now dominated by χ^-_{yxx}, is finite. The result is that for small angles of incidence the Kerr rotation will again increase. This is clearly confirmed by our experiments, but seems in contradiction with the theoretical θ_i dependence of Ref. 12. However, there one has only considered the odd component χ^-_{yzz} that also vanishes near normal incidence. At an angle of incidence of 45° the experimental and theoretical configurations should be equivalent. Here we find $\Phi_K^{(2)}=1.2°$ in excellent agreement with the theoretical prediction of 1.4° from Pustogowa and Hübner.[12] In a recent article, the latter authors have included the proper Fresnel dependence in their expression for $\Phi_K^{(2)}$, showing excellent agreement with our experimental findings.[19]

In the longitudinal configuration we also measured the wavelength dependence of both $\Phi_K^{(1)}$ and $\Phi_K^{(2)}$ at an angle of incidence of 45° (see Fig. 5). The average value for $\Phi_K^{(1)}=0.062°$, in excellent agreement with the bulk Fe value of 0.061° of Ref. 20. Figure 5 shows that in the tuning range of the Ti:sapphire laser the Kerr rotations are constant, in agreement with the theoretical prediction of Pustogowa *et al.*[12] From their calculations it follows that for $\Phi_K^{(2)}$ a strong wavelength dependence is expected above 900 nm and below 600 nm. Future experiments in these wavelength ranges are certainly desirable.

In the transversal configuration (**M** along the y axis) for p- or s-input polarization, $\chi_{ijk}=0$ for $i=y$ (see Table I). This means that the SHG signal will always be p polarized. Changing the direction of the magnetization will not affect the plane of polarization but it has an influence on the total SH signal. The magnetic contrast can be defined as

$$\rho(q_{\text{in}}q_{\text{out}})=\frac{I(2\omega,q_{\text{in}}q_{\text{out}},M^+)-I(2\omega,q_{\text{in}}q_{\text{out}},M^-)}{I(2\omega,q_{\text{in}}q_{\text{out}},M^+)+I(2\omega,q_{\text{in}}q_{\text{out}},M^-)}, \tag{6}$$

where $I(2\omega,q_{\text{in}}q_{\text{out}},M^+)$ and $I(2\omega,q_{\text{in}}q_{\text{out}},M^-)$ are the $q_{\text{in}}q_{\text{out}}$ polarized SH intensities for opposite directions of the magnetization. In Fig. 6 our results for ρ_{sp} from the uncapped Fe sample can be seen while the inset in Fig. 6 shows the experimental configuration. Similar results were obtained for the Fe/Au sample. The dependence of the angle of incidence is again easily understood with the help of Table I. For small incident angles the z component of the E vector of the SH signal will be small. This means that the odd tensor component χ^-_{xyy} will dominate, resulting in large magnetic effects. However, in the limit of normal incidence there will only be an odd contribution and no magnetic effects will be seen, as ρ depends on the interference between χ^+ and χ^-. The solid line in Fig. 6 is a theoretical fit of Eq. (6) assuming only the Fe surface to contribute to the SH signal.

III. SUMMARY AND CONCLUSIONS

In this article we have shown how the reflected SHG signal from magnetic surfaces displays nonlinear magneto-optical Kerr effects that are several orders of magnitude larger than their linear equivalents. The reasons for these

enormous enhancements are both the differences in the solutions of the e.m. wave equations as well as the differences in the symmetry properties of the nonlinear and linear optical tensors. The experimental results that have been obtained so far are in excellent agreement with the theoretical predictions (Recently, polar NOMOKE effects have also been measured).[21]

The large, interface sensitive magneto-optical effects offer great possibilities to use this nonlinear technique for studying the magnetic properties of surfaces and interfaces of very thin films and multilayers, an area of intense research nowadays.

ACKNOWLEDGMENTS

The authors are pleased to acknowledge stimulating discussions with W. Hübner. Part of this work was supported by the Stichting Fundamental Onderzoek der Materie (FOM), which is financially supported by the Nederlandse Organisatie voor Wetenschappelijk Onderzoek (NWO, and by Brite Euram II FFR CT930569.

[1] P. N. Argyres, Phys. Rev. **97**, 334 (1955).
[2] Ru-Pin Pan, H. D. Wei, and Y. R. Shen, Phys. Rev. B **39**, 1229 (1989).
[3] W. Hübner and K. H. Bennemann, Phys. Rev. B **40**, 5973 (1989).
[4] J. Reif, J. C. Zink, C. M. Schneider, and J. Kirschner, Phys. Rev. Lett. **67**, 2878 (1991).
[5] G. Spierings, V. Koutsos, H. A. Wierenga, M. W. J. Prins, D. Abraham, and Th. Rasing, Surf. Sci. **287**, 747 (1993); J. Magn. Magn. Mater. **121**, 109 (1993).
[6] O. A. Aktsipetrov, O. V. Braginskii, and D. A. Esikov, Sov. J. Quantum Electron. **20**, 259 (1990).
[7] J. Reif, C. Rau, and E. Mathias, Phys. Rev. Lett. **71**, 1931 (1993).
[8] H. A. Wierenga, M. W. J. Prins, D. L. Abraham, and Th. Rasing, Phys. Rev. B **50**, 1282 (1994).
[9] H. A. Wierenga, W. de Jong, M. W. J. Prins, Th. Rasing, R. Volmer, A. Kirilyuk, H. Schwabe, and J. Kirschner, Phys. Rev. Lett. **74**, 1462 (1995).
[10] M. Fiebig, D. Frölich, B. B. Krichevtsov, and R. V. Pisarev, Phys. Rev. Lett. **73**, 2127 (1994).
[11] B. Koopmans, M. Groot Koerkamp, Th. Rasing, and H. v.d. Berg, Phys. Rev. Lett. **74**, 3692 (1995).
[12] U. Pustogowa, W. Hubner, and K. H. Bennemann, Phys. Rev. B **49**, 10031 (1994); Appl. Phys. A **59**, 611 (1994).
[13] Th. Rasing, Appl. Phys. A **59**, 531 (1994).
[14] P. B. Johnson and R. W. Christy, Phys. Rev. B **9**, 5056 (1974); Phys. Rev. B **6**, 4370 (1972).
[15] D. E. Aspnes and A. A. Studna, Phys. Rev. B. **27**, 985 (1983).
[16] D. O. Smith, J. Appl. Phys. **36**, 1120 (1965).
[17] M. Groot Koerkamp and Th. Rasing, Surf. Sci. (to be published).
[18] H. A. Wierenga, M. W. J. Prins, and Th. Rasing, Physica B **204**, 281 (1995).
[19] W. Hübner and K. H. Bennemann (to be published).
[20] A. J. Kolk and M. Orlovic, J. Appl. Phys. **34**, 1060 (1963).
[21] M. Groot Koerkamp, A. Kirilyuk, W. de Jong, Th. Rasing, J. Ferré, J. P. Jamet, and P. Meyer, these proceedings.